Research Article

Garrett Seepersad* and Sunil Bisnath

Challenges in Assessing PPP performance

Abstract: The Precise Point Positioning (PPP) GPS data processing technique has developed over the past 15 years to become a standard method for growing categories of positioning and navigation applications. The technique relies on single receiver point positioning combined with precise satellite orbit and clock information, pseudorange and carrier-phase observable filtering, and additional error modelling. Uniquely addressed is the current accuracy of the technique, and explains the limits of performance, which will be used to define paths for future improvements of the technology.

PPP processing of over 300 International GNSS Service (IGS) stations over one week results in few millimetre positioning rms error in the north and east components and centimetre-level in the vertical (all one sigma values). These results are categorised into quality classes in order to analyse the root causes of the resultant errors: "best", "worst", multipath, antenna displacement effects, satellite availability and geometry, etc. Also of interest in PPP performance is solution convergence period. Static, conventional solutions are slow to converge, with approximately 20 minutes required for 95% of solutions to reach a horizontal accuracy of 20 cm or better.

From the above analysis, the limitations of PPP and the source of these limitations are isolated, including site displacement modelling, geometric measurement strength, pseudorange multipath and noise, etc. It is argued that new ambiguity resolution and multi-GNSS PPP processing will only partially address these limitations. Improved modelling is required for: site displacement effects, pseudorange noise and multipath, and pseudorange and carrier-phase biases. As well, more robust undifferenced carrier phase ambiguity validation and improved stochastic modelling is required for the pseudorange and carrier-phase observables to allow for more realistic position uncertainties.

***Corresponding Author: Garrett Seepersad:** Department of Earth and Space Science and Engineering, York University, Toronto, Ontario, Canada, E-mail: gseeper@yorku.ca,
http://orcid.org/0000-0002-7402-8597
Sunil Bisnath: Department of Earth and Space Science and Engineering, York University, Toronto, Ontario

Keywords: PPP, PPP accuracy, PPP convergence, PPP limitations, PPP error budget

DOI 10.1515/jag-2014-0008
Received April 02, 2014; accepted August 24, 2014

1 Introduction

PPP has become a popular technique to process data from GPS (and now GNSS) receivers by incorporating precise satellite orbit and clock corrections with these measurements along with additional error modelling within a filter to provide precise estimates of 3D position, time and atmospheric water vapour. The concept of single-receiver precise point positioning (PPP) was introduced by Héroux and Kouba [14] for processing pseudorange measurements and further elaborated by Zumberge et al. [32] as an efficient method of processing pseudorange and carrier-phase measurements from large networks of static GPS reference stations.

PPP reduces overall infrastructure costs as it enables sub-centimetre horizontal and few centimetre vertical positioning with a single dual-frequency GPS receiver, in contrast to relative GPS, RTK and network RTK that require more than one receiver. The published values by Ge et al. [10] after 24 hours of observation were 3, 4 and 8 mm in the north, east and up, respectively, which were derived from GPS data from 330 stations from DOY 106 to 119 in 2006. The published values of Ge et al. [10] were selected for comparison of the York-PPP processor as it was one of the few published papers that quantify the perfomance of PPP with a significantly large dataset.

The objective is to discuss the fundamental concepts of the PPP technique consisting of a definition of the PPP error budget and current limitations of PPP. The paper then uniquely addresses the current accuracy of float PPP, explains the limits of performance, and defines paths to improvements.

Brought to you by | York University Libraries
Authenticated
Download Date | 6/18/19 9:37 PM

2 Fundamental concepts of PPP

In single point positioning, the coordinates of a receiver at an "unknown" point are sought with respect to a geodetic datum by using the "known" positions and clock offsets of the GNSS satellites being tracked. Single point positioning (also referred to as absolute positioning or point positioning) is the most basic GPS solution obtained with epoch-by-epoch least-squares estimation. For point positioning, GPS provides two levels of services, the Standard Positioning Service (SPS) with access for civilian users and the Precise Positioning Service (PPS) with access for authorized users. In SPS, only the single-frequency C/A-code is currently available, which provides to the GPS user an accuracy standard of ~10 m 95% confidence level [5]. The accuracy performance standard of GPS is based on healthy SPS satellite information system, neglecting single-frequency ionospheric delay model errors and includes group delay time correction (TGD) and inter-signal bias (P(Y)-code to C/A-code) errors on L_1 [5]. GPS SPS users can also use services such as Wide-Area Augmentation System (WAAS) to improve their horizontal and vertical accuracy to ≤1.5 m and ≤2 m respectively, at a confidence level of 95% [8].

Similar to single point positioning, PPP allows for the estimation of a state space solution using undifferenced GPS observations collected using a single GPS receiver. The wide adoption of PPP became a possibility with the development of high-rate precise orbits and clocks. The IGS GPS final orbit accuracy in 2013 was on the order of 2.5 cm. GPS satellites carry highly stable atomic clocks to generate accurate timing signals. Although the onboard atomic clocks are stable, the inability of the onboard oscillator to maintain synchronisation with GPS time results in a clock error. The deviation between the atomic time and GPS time is known as the satellite clock error [31]. The GPS clock rms error is ~75 ps with a standard deviation of ~20 ps [15] where the standard deviation is calculated by removing the inherent bias and drift.

It is necessary when processing data with a PPP algorithm to mitigate all potential error sources in the system. As a result of the un-differenced nature of PPP, all errors caused by the space segment, signal propagation and signal reception directly impact the positioning solution. Error mitigation can be carried out by modelling, estimating or elimination through observable linear combinations. Figure 1 directly compares the approaches of SPP and PPP for GPS, but they are also directly applicable to all GNSSs. In the SPS of GPS, metre-level real-time satellite orbit and clock information is supplied to the user by each GPS satellite. For single-frequency users, ionospheric refraction information is also required. All of this information is combined with C/A-code pseudorange measurements to produce metre level user position estimates[2].

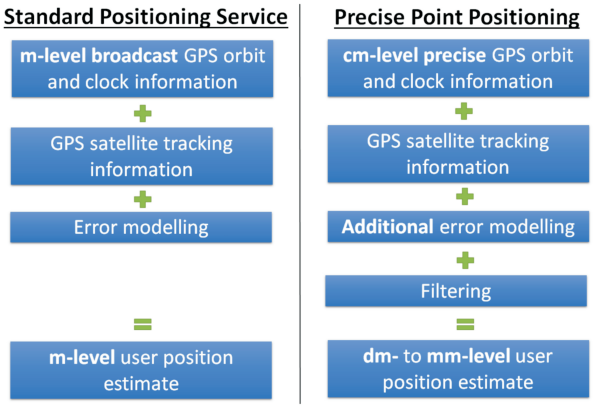

Fig. 1. Fundamental idea underlying the SPS technique as compared to PPP.

2.1 Challenges in defining PPP error budget

Each GNSS has been designed to perform with a high level of precision. However, there still remains numerous errors sources to be accounted for in the pseudorange or carrier-phase observations to eliminate effects such as special and general relativity, Sagnac delay, satellite clock offsets, atmospheric delays, etc. These errors can cause a combined deviation of +/- 50-100 m in the range and must be considered even for single point positioning.

When attempting to combine satellite positions and clocks precise to a few centimetres with ionospheric-free pseudorange and carrier-phase observations, it is important to account for some effects that may not have been considered in SPS. Also, defining this error budget becomes more challenging as these error sources can be subdivided into errors projected onto the range and localized antenna displacements. This situation is illustrated in Figure 2. As the signal is transmitted from the satellite to the receiver, error sources affected in the range domain include satellite and receiver clock error, atmospheric, relativistic, multipath and noise and carrier-phase wind-up. Antenna displacement effects occur at the satellite and receiver and these include effects such as phase centre offset and variation, orbit and at the receiver, site displacement effects such as solid Earth tides and ocean loading.

Brought to you by | York University Libraries
Authenticated
Download Date | 6/18/19 9:37 PM

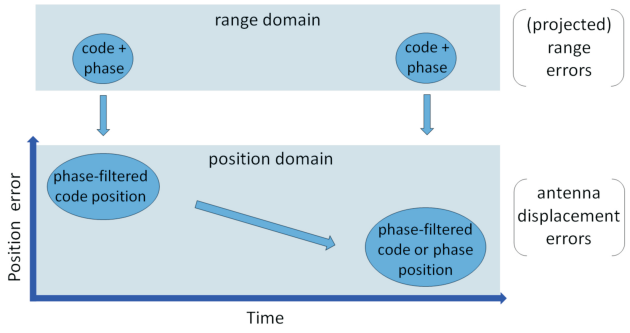

Fig. 2. Range to position and time domain transformations in PPP data processing illustrating the different domains of PPP error sources.

2.2 PPP error management

As previously mentioned, there are additional corrections which have to be applied to pseudorange and carrier-phase measurements such as phase wind-up, antenna phase centre offset and geophysical effects, in addition to other commonly known effects such as relativistic correction in order to have a complete observation model in PPP. The un-differenced observation equations can be written as follows, where the pseudorange measurement in eq'n 1 is measured in units of distance and the carrier-phase measurement in eq'n 2 is measured in units of cycles which is converted to distance [17, 18, 32].

$$P_{L_i} = \rho + c(dr - dT) + d_{orb} + d_{iono} + d_{tropo} + d_{multi(P_{L_i})} + b^r_{P_{L_i}} - b^s_{P_{L_i}} + \varepsilon(P_{L_i}) \quad (1)$$

$$\phi_{L_i} = \rho + c(dr - dT) + d_{orb} - d_{iono} + d_{tropo} + \lambda_{L_i} N_{L_i} + d_{multi(\phi_{L_i})} + b^r_{\theta_{L_i}} - b^s_{\theta_{L_i}} + \varepsilon(\theta_{L_i}) \quad (2)$$

where P_{L_i} - measured pseudorange on $L_{1|2}$ (m), ϕ_{L_i} - measured carrier-phase range on $L_{1|2}$ (m), ρ - true geometric range (m), c - speed of light (ms^{-1}), dt - receiver clock error (s), dT - satellite clock error (s), d_{orb} - satellite orbit error (m), d_{iono} - ionospheric delay (m), d_{trop} - tropospheric delay (m), λ_{L_i} - wavelength on $L_{1|2}$, N_i - non-integer phase ambiguity on $L_{1|2}$ (cycle), $d_{multi(P_{L_i})}$ - pseudorange multipath effect on $L_{1|2}$ (m), $d_{multi(\theta_{L_i})}$ - carrier-phase multipath on $L_{1|2}$ (m), $b^\star_\star$ - hardware biases (m), $\varepsilon(\star)$ - measurement noise (m).

The following subsections provide an overview of some of the more prominent error sources that has to be accounted for in PPP and Table 1 is a summary of all corrections accounted for and the applied mitigation strategy.

2.2.1 Ionospheric refraction

The ionospheric delay is greater at the L_2 carrier frequency than that of the L_1 carrier frequency. Up to 99.9% of the ionospheric delay can be eliminated through linear combination of GPS observables on L_1 and L_2 frequencies [4, 13]. Hernández-Pajares et al. [12] and Elsobeiey et al [7] showed that neglecting the second-order ionospheric delay can introduce an error of order of up to 2 cm. A negative side effect of the iono-free combination is the measurement noise is approximately tripled versus the noise on L_1 or L_2 [20].

2.2.2 Tropospheric refraction

The troposphere consists of the dry or hydrostatic component which represents approximately 90% of the delay and the remaining 10% consists of the wet component. The tropospheric delay at sea level is of the order of ~2.5 m at the zenith, to over 20 m at elevation angles less than 15° [21]. The zenith wet tropospheric delay, however, may vary from a few millimetres to as much as 40 cm. The accuracy of the hydrostatic zenith delay is at the millimetre level, while the wet delay is calculated with an error of a few centimetres. If the atmospheric pressure measurement is available, the hydrostatic delay is fixed and the wet delay is estimated [18, 25].

2.2.3 Multipath and noise

Multipath occurs when signals travelling from a transmitter to a receiver propagate via multiple paths due to reflection and diffraction. The multipath effect produces errors in both pseudorange and carrier-phase measurements. The magnitude of range error can reach up to 10 to 20 metres for pseudorange measurements and up to 5 cm for carrier-phase measurements [31]. Mitigative strategies include cautious antenna placement (by selecting of low-multipath environment for antenna placement), hardware solutions (such as extended ground planes and choke rings), software solutions (satellite elevation angle masks and Hatch filtering) and hybrid solutions (which are a combination of hardware and software components).

2.3 Limitations of PPP

While PPP presents definite advantages, there are still underlying limitations, which are the focus of most current PPP research activities.

Brought to you by | York University Libraries
Authenticated
Download Date | 6/18/19 9:37 PM

Table 1. Summary of error sources in PPP, mitigative strategy and residual error.

Effect	Magnitude	Domain	Mitigation method	Residual error
Ionosphere	10s m	range	linear combination	few mm
Troposphere	few m	range	modelling; estimation	few mm
Relativistic	10 m	range	modelling	mm
Sat phase centre; variation	m - cm	pos; range	modelling	mm
Pseudorange multipath; noise	1 m	range	filtering	10s cm - mm
Solid Earth tide	20 cm	position	modelling	mm
Carrier-phase wind-up (iono-free)	10 cm	range	modelling	mm
Ocean loading	5 cm	position	modelling	mm
Satellite orbits; clocks	few cm	pos; range	filtering	cm - mm
Carrier-phase multipath; noise	1 cm	range	filtering	cm - mm
Rcv phase centre; variation	cm - mm	pos; range	modelling	mm
Pole tide	few cm	position	modelled	mm
Receiver clock	10s m	range	estimated	mm
Atmospheric loading	cm - mm	position	modelling	cm - mm
Pseudorange biases	60 cm	range	modelling	mm
Ambiguity term	m - cm	range	estimated	mm

2.3.1 Convergence

PPP requires a relatively long initialization period of a few tens of minutes at least for the carrier-phase ambiguities to converge to constant values and for the solution to reach its optimal precision. Convergence is primarily caused by the estimation of the carrier-phase ambiguities initially from the relatively noisy pseudoranges. The pseudorange measurements are approximately 100 times less precise than carrier-phase measurements. Initialization of the carrier-phase ambiguities by the pseudorange allows PPP to take full advantage of the precise but ambiguous carrier-phase observations; however, the length of time it takes to reach the optimal solution is a major disadvantage to the wider use of the technique. If the pseudoranges were more precise there would be a reduction in the convergence period [29]. Ambiguity resolution in PPP (PPP-AR) requires the equipment delays within the GPS measurements to be mitigated, which would allow for resolution of the integer nature of the carrier-phase measurements [4, 10, 19]. PPP-AR would accelerate the overall solution convergence to give cm-level horizontal accuracy after 1 hour or less. Collins et al. [4] and Laurichesse et al. [19] saw improvements in hourly position estimates by 2 cm and Geng et al. [11] saw noticeable hourly improvements from 1.5, 3.8 and 2.8 cm to 0.5, 0.5, 1.4 cm for north, east and up, respectively.

2.3.2 Pseudorange multipath and noise

Pseudorange multipath and noise together are the largest remaining unmanaged error source in PPP. By reducing the effects of the multipath and noise on the pseudorange observables, the carrier-phase ambiguities will reach a steady state at an earlier time, thus reducing the initial and re-convergence period of PPP as well as decreasing the time required for PPP-AR to resolve ambiguities [28].

2.3.3 Integrity monitoring

While much research effort has been applied to improving the accuracy of PPP coordinate solutions and the duration of data collection needed to achieve such accuracies, little work has been published on the integrity of PPP solutions. Integrity is the measure of the trust that can be placed in the information supplied by a navigation system [24]. Integrity monitoring also includes the ability of the system to provide timely warnings to users when the system should not be used for navigation. Providing integrity information for PPP single receiver estimates is all that more important as all parameters have to be accounted for, unlike other processing techniques that have additional redundancy of other receivers such as double-differenced static, multi-baseline networks and network RTK. Post-fit residuals from PPP epoch solutions could be analysed to detect individual measurement outliers, or more significant problems. Aside from measurement outlier detection, the

Brought to you by | York University Libraries
Authenticated
Download Date | 6/18/19 9:37 PM

covariance of the estimated position is the main indicator of the solution accuracy in PPP, as a reference solution may not always be available. There have been very few studies that address this integrity monitoring in PPP to answer the questions: How accurate is my epoch PPP position? And, how realistic is the internal PPP uncertainty estimate [28]?

2.3.4 Quality and consistency of models

In PPP, undifferenced GPS observations are collected using a single dual-frequency GPS receiver. As a result, error sources such as tidal loading, carrier-phase wind-up, antenna phase offset and clock errors to be accurately accounted for, as opposed to (short baseline static) relative positioning, as these errors are eliminated through measurement differencing. There is a requirement for these models to perform exceedingly well to assure the highest accuracy is provided to the user. This requirement is a challenging task, as error sources should be properly modelled. Also, consistency between the models used in the generation of GPS orbit and clock products and those used in the PPP user algorithm will aid in the minimization of position solution errors.

3 Examining current accuracy and limitations of PPP

This section quantifies the current accuracy and convergence of PPP in static and kinematic processing modes for a very large set of globally distributed sites. These experiments are followed by analysis of the global distribution of horizontal and vertical position biases of all processed sites. Also, a unique analysis of how PPP position biases and convergence vary within a small geographical region and possible causes is provided.

3.1 Dataset and processing parameters

GPS data from 300 IGS stations observed during DOY 183 to 189, GPS week 1695, of 2012 were processed using the York-PPP software [29]. York-PPP was developed based on the processing engine used by the on-line CSRS-PPP service [23]. The sites chosen were a subset of those processed regularly by most IGS ACs, representing a good global distribution. The distribution of the sites is illustrated in Figure 3. Dual-frequency receivers tracking either the C/A or P(Y) - code on L_1 were used. For receivers that do not record

Fig. 3. Global distribution of the selected 300 IGS stations observed during DOY 183 to 189, GPS week 1695, of 2012.

the P1 observable, the P1C1 pseudorange bias correction was applied. Settings used for the evaluation include the ionosphere-free combination of L_1 and L_2 data, 2 m and 15 mm a priori standard deviations for pseudorange and carrier-phase observations, respectively, and a 10° elevation cut-off angle.

IGS final 5 minute orbit and 30 second clock products were used. The reference stations were analysed in static mode. Receiver clocks were estimated epoch-by-epoch. The zenith tropospheric delays were also estimated each epoch with a random walk co-efficient of 2 cm/sqrt (hour). The station coordinates were initialized using a pseudorange only solution with an initial constraint of 10 m. The IGS absolute antenna model file was used and ocean loading coefficients were obtained from Scherneck [26] for each of the sites processed.

3.2 Conventional static PPP results

The primary factor affecting the convergence period of PPP is the quality of the pseudorange measurements as the initial solution is a pseudorange only solution. The accuracy of PPP is due to the limited precision of the current precise orbit and clock products and the quality of the models used for atmospheric modelling (primarily the estimation process of the zenith tropospheric delay), the solid Earth tides and ocean loading and pseudorange and

Brought to you by | York University Libraries
Authenticated
Download Date | 6/18/19 9:37 PM

Table 2. Final solution produced by York-PPP from 24 hour datasets from 300 sites for DOY 183-189, processed in static mode for a total sample size of 2010. All units are in millimetres.

	max	mean	std dev	rms
Northing	27	-1	5	5
Easting	26	-1	6	6
Horizontal	28	1	7	7
Vertical	51	-1	13	13
3D	52	2	15	15

carrier-phase multipath and noise. To quantify the accuracy of PPP, the estimated positions were compared with the weekly SINEX solution provided by the analysis centres [3]. Solution here refers to the estimated position generated after processing the entire 24 hour dataset. The error term represents the difference between the estimated PPP solution and the IGS SINEX solution. The distribution of the error in the horizontal and vertical components is illustrated in Figure 4 and Figure 5, respectively, with histogram bin sizes of 2 mm and 5 mm, respectively, for a sample size of 2100.

PPP is capable of producing sub-centimetre accuracy in the horizontal component and centimetre in the vertical. 99% of the data processed had an error in the horizontal component of less than or equal to 25 mm and 87% of the results had a horizontal error of less than one centimetre. In the vertical component, 99% of the data processed had an error of less than 80 mm and 95% of the results had an error less than 50 mm. It is expected for the vertical component to be of a lesser accuracy than that of the horizontal component due to satellite geometry which is inherent to all modes of GPS data processing and the quality of the models used for atmospheric modelling, primarily the estimation of the zenith tropospheric delay as well as the solid Earth tides and ocean loading. A summary of the statistics for positions estimated is presented in Table2. The overall solution had an rms of 5, 6 and 13 mm in the north, east and up, respectively.

The published values by Ge et al. [10] were 3, 4 and 8 mm in the north, east and up, respectively. The difference in the rms performance is possibly due to Ge et al.'s application [10] of a 7-parameter Helmert transformation when comparing their results against the IGS SINEX coordinates. The 7-parameter Helmert transformation between the two products allows the removal of systematic differences caused by reference frame realizations that are slightly different [22]. The Helmert transformation is not required to be carried out as the solutions produced would have been in the same coordinate system as the IGS weekly

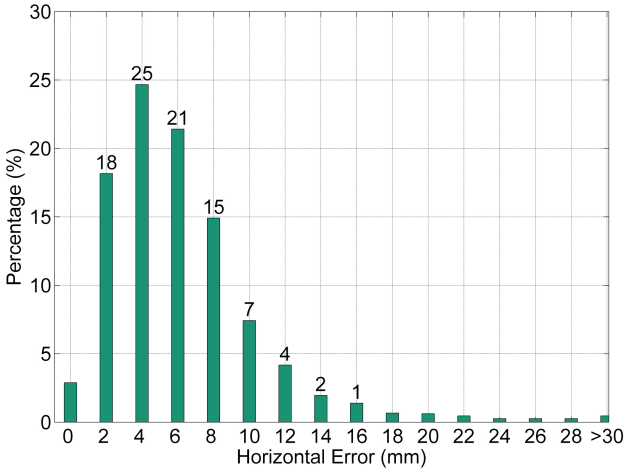

Fig. 4. Histogram showing distribution of the horizontal component with a bin size of 2 mm produced by York-PPP from 24 hour datasets from 300 sites for DOY 183-189, processed in static mode for a total sample size of 2010.

satellite orbit and coordinate products. Due to the acceptance of PPP to a broader spectrum of applications, it is useful to examine PPP without applying such transformations after processing. Some users may not have the resources or skillset to apply Helmet transformation, and if PPP is to be used to directly access the GPS (GNSS)-base reference frame, then such transformations should not be necessary.

Point positioning is calculated relative to a well-defined global reference system, in contrast to relative positioning, where the coordinates are in relation to some other fixed point. Eckl et al. [6] describes the accuracy of static relative positioning with a geodetic-grade receiver as typically 5 mm + 0.5 ppm (rms) for the horizontal component and 5 mm + 1 ppm (rms) for the vertical component. These values represent the highest accuracy possible for static relative positioning, as the fixed point would have an uncertainty associated with it and the quality of

Brought to you by | York University Libraries
Authenticated
Download Date | 6/18/19 9:37 PM

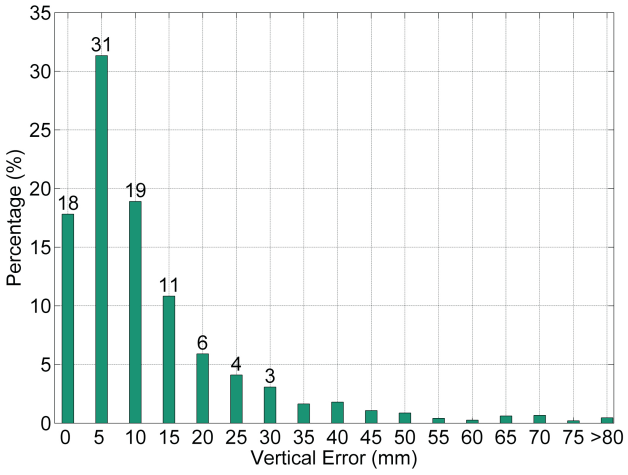

Fig. 5. Histogram showing distribution of the absolute error in the vertical component with a bin size of 5 mm produced by York-PPP from 24 hour datasets from 300 sites for DOY 183-189, processed in static mode for a total sample size of 2010.

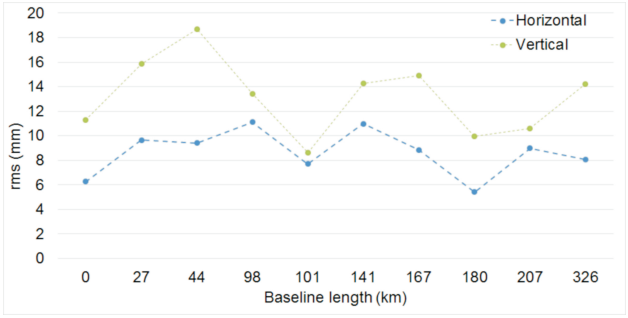

Fig. 6. Rms values at different baseline length for the horizontal and vertical components.

the estimated solution would deteriorate as the baseline length increases. To determine if it is possible to replace static relative positioning with PPP, relative difference between 10 sets of stations were calculated using the estimated PPP solution for DOY 183 to 189 and compared to the relative difference calculated using the IGS SINEX solution. The rms values for the horizontal and vertical components at varying baseline lengths are illustrated in Figure 6. To determine static relative error statistics, the solution estimates from the York-PPP software were compared to the specifications published by Eckl et al. [6]. In the horizontal component, the PPP solution had an accuracy of 8 mm, which is comparable to static relative positioning. In the vertical component, the accuracy of relative positioning is 2.6 times greater than that of the PPP solution. The accuracy of the relative difference calculated from the estimated PPP solution is reliant on how precisely station dependent error sources are mitigated, rather than sensitivity of base line length, as is the case of relative positioning.

3.3 Conventional kinematic PPP results

The difference between static and kinematic mode in PPP primarily exists in the variation of the process noise models in the sequential least-squares (in this case) or Kalman filter. The process noise for the coordinates serves as a priori weighted constraints to the parameters. The quantity of process noise can be scaled based on the user dynamics such as stationary, walking, driving and satellite motion to simulate the receiver. A process noise of 10 m/s, equivalent to that of a terrestrial vehicle in motion was used, even though overly pessimistic, it serves to better analyse the contrast in the quality of the results from static and kinematic mode and the variation of convergence.

To examine the kinematic mode of the software, the same static dataset was used to simulate kinematic data. This method of analysis was chosen due to the limited availability of reference solutions for kinematic results with a higher precision than PPP. Presented in Figure 7 and Figure 8 are the horizontal and vertical kinematic results, respectively. In the horizontal component, 98% of the data processed had an error of less than 150 mm and 95% had an error of less than 80 mm. In the vertical component, 99% of the data processed had an error less than 400 mm and 95% had an error of less than 160 mm.

A summary of the statistics of positions estimated is presented in Table 3. In static mode, the horizontal component rms was 7 mm in contrast to kinematic mode which was 46 mm, and in the vertical component 13 mm in static mode and 72 mm in kinematic mode. The solution quality deteriorated because of the magnitude of the process noise used, adding large uncertainties to each parameter, allowing the solution to converge freely based on individual measurements, whereas in static mode the parameters are tightly constrained, thus a significantly higher accuracy of results is achieved through the power of averaging. It cannot be overstated that these kinematic results are therefore quite conservative.

3.4 Convergence period in static and kinematic mode

PPP definitely presents advantages for many applications in terms of operational flexibility and cost-effectiveness.

Brought to you by | York University Libraries
Authenticated
Download Date | 6/18/19 9:37 PM

Table 3. Final solution produced by York-PPP from 24 hour datasets from 300 sites for DOY 183-189, processed in kinematic mode for a total sample size of 2010. All units are in millimetres.

	max	mean	std dev	rms
Northing	285	3	27	27
Easting	365	-2	37	37
Horizontal	463	4	46	46
Vertical	592	-4	72	72
3D	752	6	85	85

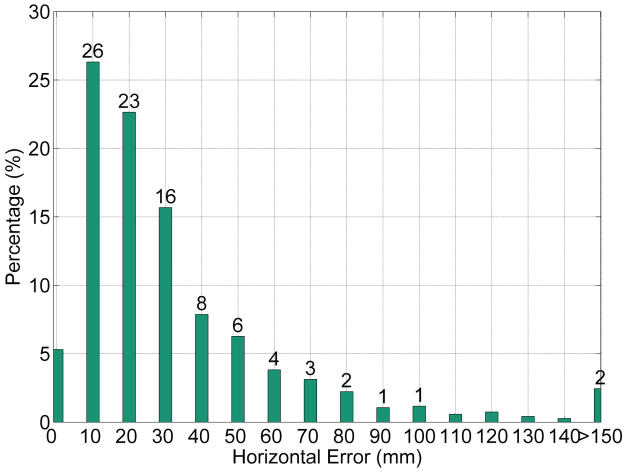

Fig. 7. Histogram showing distribution of the horizontal component with a bin size of 10 mm produced by York-PPP from 24 hour datasets from 300 sites for DOY 183-189, processed in kinematic mode for a total sample size of 2010.

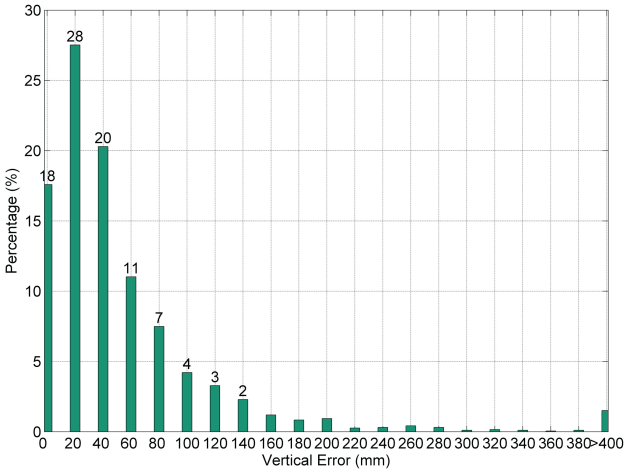

Fig. 8. Histogram showing distribution of the absolute error in the vertical component with a bin size of 20 mm produced by York-PPP from 24 hour datasets from 300 sites for DOY 183-189, processed in kinematic mode for a total sample size of 2010.

PPP convergence depends on a number of factors such as the number and geometry of visible satellites, user environment and dynamics, observation quality and sampling rate [1]. As these different factors interplay, the period of time required for the solution to reach a pre-defined precision level will vary.

A horizontal threshold of 20 cm was set to examine the amount of time required for 95% of the data processed to attain this pre-defined threshold. A threshold of 20 cm was selected as this specification is utilized in a variety of commercial applications such as offshore positioning for hydrography (dynamic positioning, construction, etc.) [16], precision agriculture [30], and airborne mapping for aircraft / camera sensor positioning [9]. For Geodetic control surveying more stringent specifications are required [9].

The variation in convergence period is easily visible between static and (conservative) kinematic modes as a result of the difference in the process noise applied. In static mode, the estimated parameters are constrained, allowing the float ambiguities to be estimated within a shorter time period. In static mode, an exponential trend was observed in contrast to the quasi-linear trend in kinematic mode, as illustrated in Figure 9. In static mode, 25% of the solutions had an initial horizontal error of 20 cm or less, and 20% in kinematic mode. Within 10 minutes 85% of data processed had met the horizontal accuracy threshold in static mode. An additional 10 minutes was required for 95% of the data to converge. It took approximately 25 minutes for 75% of the solutions to converge in kinematic mode and 55 minutes for 89% of the solutions.

For various commercial applications described, it would be recommended to collect an initial 20 minutes of data while the receiver is stationary, after which, the processing mode can be changed to kinematic and the receiver can be moved to collect data at various locations. The initial 20 minutes can be processed in static mode al-

Brought to you by | York University Libraries
Authenticated
Download Date | 6/18/19 9:37 PM

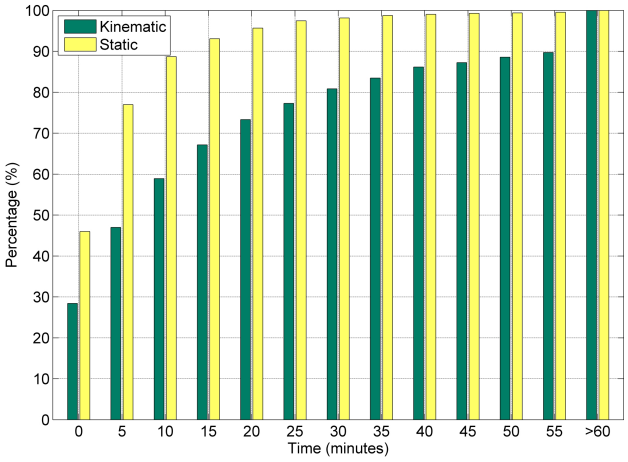

Fig. 9. Cumulative histogram showing convergence period to a predefined horizontal threshold of 20 cm for static and kinematic PPP produced by York-PPP from 300 sites for DOY 183-189, a total sample size of 2010 for each processing mode.

lowing solution to converge within a shorter time period, after which the processing is switched to kinematic and the receiver moved.

3.5 Geographic distribution of position biases

Position repeatability can quantitatively reflect the intrinsic positioning quality of PPP. The position repeatability was generated by computing the station-specific positions over one week and then compared to the IGS SINEX solution. The geographical distribution of the average station-specific absolute position differences in the horizontal and vertical components is illustrated in Figure 10 and Figure 11, respectively. Overall, in the horizontal component all stations had a bias of 1 mm in the horizontal and -1 mm in the vertical when processed in static mode. In the horizontal component, no visible trends are noticed when the weekly average for each site is examined. In the vertical component, the absolute bias is examined. In the horizontal component, 87% of the data had an error of less than one centimetre in contrast to vertical component, where only 67% of the data had an error less than one centimetre. The vertical biases greater than 3 cm, were primarily isolated to coastal regions, this could have been due to limitations of the ocean loading corrections.

To further highlight the variations of PPP solution, Figure 12 contains 5% of the "best" and "worst" horizontal solutions. The figure dramatically shows how accurate the

Table 4. Summary of the position difference of the "best", "average" and "worst" datasets on DOY 186, 189 and 189 respectively. Bias and standard deviation of the solution from DOY 183 – 189 include for comparison. All units are in millimetres.

Site		Horizontal	Vertical
RIGA	Weekly	3 +/- 2	3 +/- 5
	DOY: 186	0	1
CONT	Weekly	9 +/- 2	-11 +/- 2
	DOY: 189	5	-6
POVE	Weekly	29 +/- 10	-1 +/- 10
	DOY: 189	39	-12

"best" solutions are, with virtually no bias or variance, while the "worse" solutions contain centimetre level dispersion. Further analysis is required to determine if there is a root cause or causes of these solution variations, or if the variations reflect the limits of the processing technique. Figure 13 illustrates the geographical distribution "best" and "worst" 5% of horizontal solutions highlighted in blue and red respectively. The "worst" datasets are most noticeable in regions where the IGS has a weaker densification of continuously operating reference stations and around coastal regions. To further quantify the distinction between the "best" and "worst" horizontal solutions, the sites were further examined with respect to the number of satellites, position dilution of precision (PDOP), monument receiver, antenna and clock type. No noticeable trends were observed. In areas such as South America, Asia and southern Africa that do not have as high a station density as North America and Europe, the observation geometry may not be as strong for the determination of orbit and clock products. Also, some South American stations may been affected by more active ionospheric conditions.

Of the 2100 different datasets processed, the "best", "average" and "worst" datasets were selected based on the quality of the horizontal position for further analysis. The convergence for northing, easting and up components for each dataset is presented in Figure 14, Figure 15 and Figure 16. Table 4 is a summary of the statistics for each of the three sites. The statistics consists of the DOY which had the "best", "average" and "worst" solution as well as the mean and standard deviation for all stations processed from DOY 183 to 189.

The dataset from the site RIGA on DOY 186, located in Latvia, Northern Europe had the best horizontal solution for all datasets processed, with a horizontal and vertical difference of 0 and 1 mm, respectively. The weekly solution had an average difference of 3 mm and standard deviation of 2 mm in the horizontal and an average difference of 3 mm and standard deviation of 5 mm in the vertical. The

Brought to you by | York University Libraries
Authenticated
Download Date | 6/18/19 9:37 PM

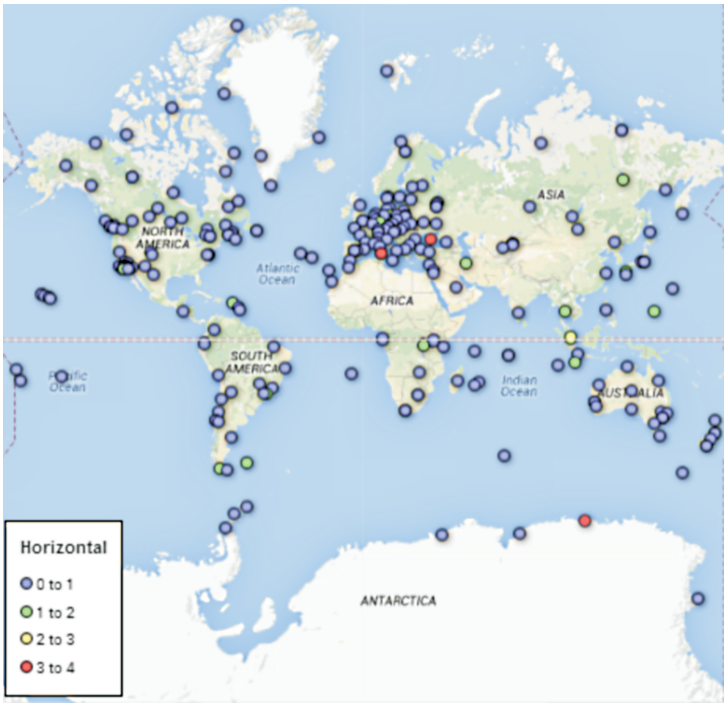

Fig. 10. Geographical distribution of the station-specific position differences in the horizontal component processed in static mode by York-PPP from 24 hour datasets from 300 sites for GPS week 1695. All units are in cm.

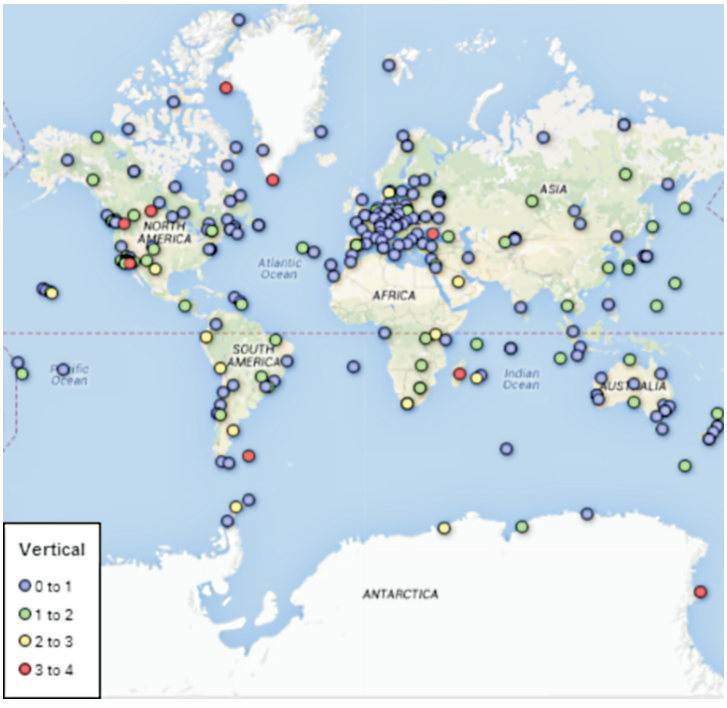

Fig. 11. Geographical distribution of the station-specific absolute position differences in the vertical component processed in static mode by York-PPP from 24 hour datasets from 300 sites for GPS week 1695. All units are in cm.

Brought to you by | York University Libraries
Authenticated
Download Date | 6/18/19 9:37 PM

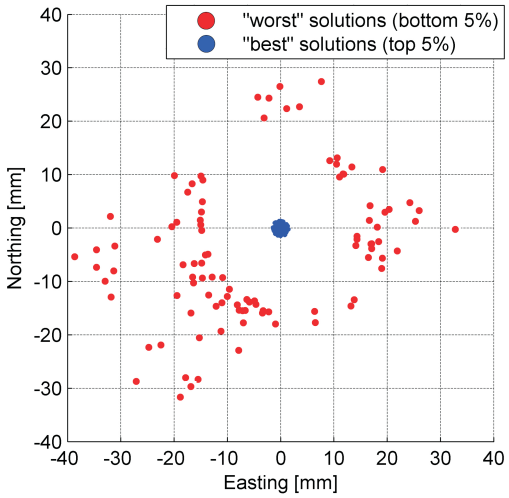

Fig. 12. "Best" and "worst" 5% of PPP horizontal solutions as compared to weekly IGS SINEX solution produced by York-PPP from 24 hour datasets from 300 sites for DOY 183-189, processed in static mode for a total sample size of 2010.

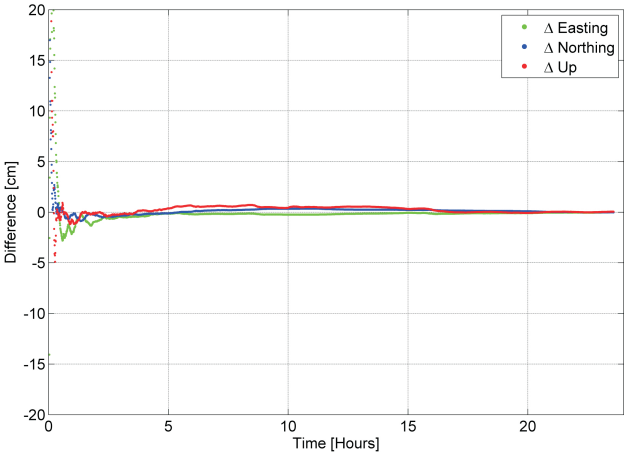

Fig. 14. Site RIGA from DOY 186 of 2012 showing "best" convergence solution in static mode with a convergence time of 5 minutes to a pre-defined horizontal threshold of 20 cm with a horizontal and vertical difference of 0 and 1 mm, respectively.

Fig. 13. Geographical distribution of the "best" and "worst" 5% of PPP horizontal solutions as compared to weekly IGS SINEX solution highlighted in blue and red, respectively.

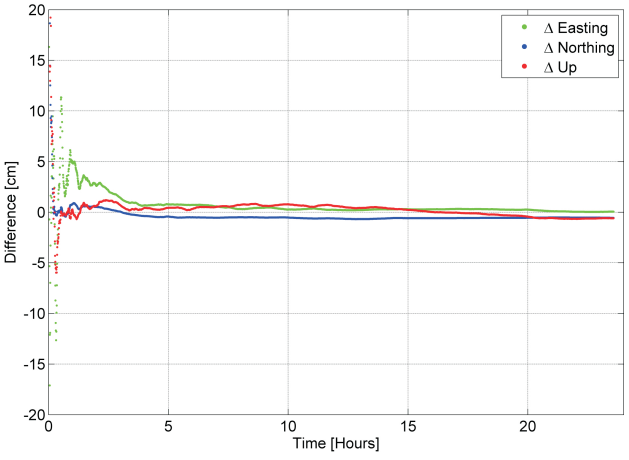

Fig. 15. Site CONT from DOY 189 in 2012 showing "average" convergence solution in static mode with a convergence time of 15 minutes to a pre-defined horizontal threshold of 20 cm with a horizontal and vertical difference of 5 and -6 mm, respectively,

Brought to you by | York University Libraries
Authenticated
Download Date | 6/18/19 9:37 PM

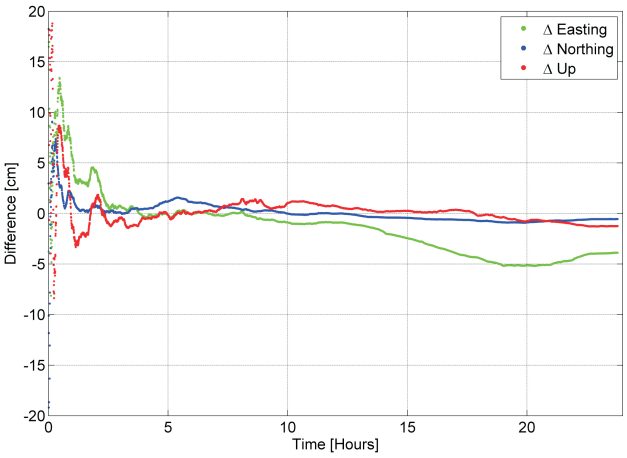

Fig. 16. Site POVE from DOY 189 of 2012 showing "worst" convergence solution in static mode with a convergence time of 20 minutes to a pre-defined horizontal threshold of 20 cm with a horizontal and vertical difference of 39 and -12 mm, respectively.

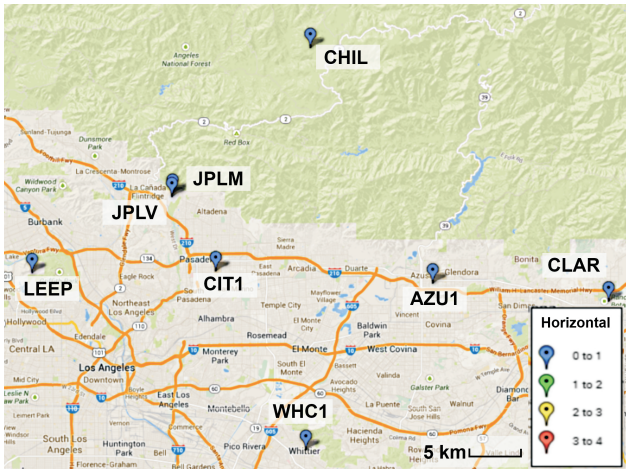

Fig. 17. Geographic distribution of the average horizontal position difference from DOY 183 – 189 for the selected 8 IGS sites within the city of Los Angeles. All units are in centimetre.

solution achieves a steady state of 20 cm horizontal within the first 5 minutes.

The dataset from the site CONT, located in Concepcion, Chile on DOY 189 performed average with a horizontal and vertical difference of 5 and -6 mm, respectively. The weekly solution had an average difference of 9 mm and standard deviation of 2 mm in the horizontal and an average difference of -11 mm and standard deviation of 2 mm in the vertical. The solution achieves a steady state of 20 cm horizontal within the first 15 minutes.

The dataset from the site POVE on DOY 189, had the worst horizontal solution of all the datasets processed. The site is located in Porto Velho, Brazil. The dataset had a horizontal and vertical difference of 39 and 12 mm, respectively. The weekly solution had an average difference of 29 mm and standard deviation of 10 mm in the horizontal and an average difference of -1 mm and standard deviation of 10 mm in the vertical. The solution achieves a steady state of 20 cm horizontal within the first 20 minutes. A few centimetre divergence is noted only in the east component with sub-centimetre accuracy in the north component and centimetre-level in the up component. This may be due to undetected cycle slips which can be expected in regions with high ionospheric activity, such as South America. POVE also had the least stable convergence of the three sites. This may be due to a weak estimation of the wet component of the tropospheric delay as in areas such as South America the wet delay is also highly variable. A more detailed analysis is required in order to isolate the cause or causes of the large PPP positioning errors present at POVE DOY 189 of 2012.

3.6 Analysis of varying convergence and position biases

As previously discussed, PPP convergence is affected by several different factors. To better understand the factors affecting convergence, 8 active control points were selected within the city of Los Angeles. This area was selected because of the dense network and varying position quality amongst the stations. The number of satellites, GDOP, pseudorange multipath and noise, pseudorange residuals, receiver, antenna, clock and monument type were analyzed to better understand the varying rates of convergence and varying position quality within the relatively small geographic region of 900 km^2. Summarized in Table 5 is the monument description and receiver, antenna and clock type for each of the stations.

Illustrated in Figure 17 and Figure 18 is the geographic distribution of the averaged difference between the estimated PPP solution from the IGS SINEX solution from DOY 183 to 189 for the horizontal and vertical components. In the horizontal component all the sites had an error of less than 1 cm. In the vertical component, centimetre differences were observed. In the vertical component, sites such as JPLM, JPLV, AZU1 and WHC1 performed above average as biases were less than one centimetre.

Brought to you by | York University Libraries
Authenticated
Download Date | 6/18/19 9:37 PM

Table 5. Summary of the position difference of the "best", "average" and "worst" datasets on DOY 186, 189 and 189 respectively. Bias and standard deviation of the solution from DOY 183 – 189 include for comparison. All units are in millimetres.

Site	Receiver	Antenna	Clock	Monument Description
AZU1	TRIMBLE NETRS	ASH701945B_M	Internal	shallow rod
LEEP	TPS NET-G3A	ASH700936A_M	Internal	shallow rod
CLAR	TPS NET-G3A	TPSCR.G3	Internal	shallow rod
CHIL	TPS NET-G3A	TPSCR.G3	Internal	rock-pin/metal-tripod
JPLM	ROGUE SNR-8100	AOAD/M_T	Rubidium	brass plate
JPLV	JPS EGGDT	JPLD/M_R	Rubidium	brass plate
CIT1	AOAD/M_T	Trimble NETRS	Internal	wall
WHC1	TPS NET-G3A	TPSCR.G3	Internal	pillar

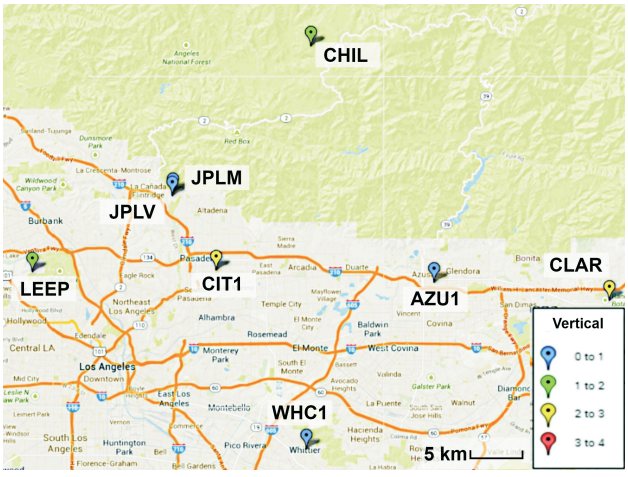

Fig. 18. Geographic distribution of the average vertical position difference from DOY 183 – 189 for the selected 8 IGS sites within the city of Los Angeles. All units are in centimetre.

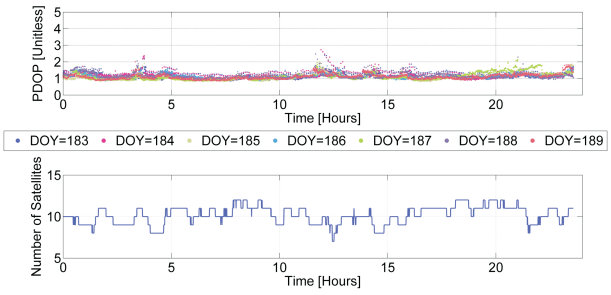

Fig. 19. The PDOP (upper plot) and the number of satellites (lower plot) for DOY 183-189 of 2012 for the site CIT1.

The PDOP and number of satellites for the sites CIT1 and JPLM are illustrated in Figure 19 and Figure 20 respectively. CIT1 and JPLM were selected as they were within 5 km of each other, this would allow for both stations to be under similar ionospheric conditions. The average position difference of CIT1 was 2 cm greater than that of JPLM in the vertical component. The PDOP of JPLM was greater than that of CIT1 with a standard deviation of 1.3 and 1, respectively. The spikes in the PDOP at the site JPLM was due to relatively low number of satellites with a minimum of 5 and maximum of 8 in contrast to CIT1, which had a minimum of 8 and maximum of 12. CIT1 is located on the California Institute of Technology which has clear sky coverage in contrast to JPLM, which has a lesser number of satellites as it is located south-west of a national forested area with an altitude ranging from 372 m (altitude of JPLM) to 1567 m (altitude of CHIL). While the site CIT1 had a lower PDOP and more satellites indicating a strong satellite geometry, the quality of data from the site JPLM provided a better solution quality indicating that more satellites and a strong geometry may not always provide a higher quality solution.

The term convergence in this analysis refers only to the initial 2 hours of PPP processing, as the final solution of all the sites met the expected accuracy of PPP. The weekly convergence trends of all 8 sites were examined; AZU1 and CLAR had the worst convergence and LEEP had below average quality of convergence. All the other sites showed good convergence where a steady state was attained within the first 30 minutes of processing. Presented in Figure 21 and Figure 22 is the horizontal convergence for the sites AZU1 and WHC1 illustrating the worst and best convergence, respectively.

To quantify the magnitude of multipath present at each site, the so-called pseudorange multipath observable is computed [13]. A linear combination of the pseudorange and carrier-phase measurements is used. By convention, the carrier-phase multipath and noise, approximately two orders of magnitude smaller than the pseudorange multipath and noise, are neglected in this calculation. The estimate of pseudorange multipath and noise on L_1 (mp_1) is

Brought to you by | York University Libraries
Authenticated
Download Date | 6/18/19 9:37 PM

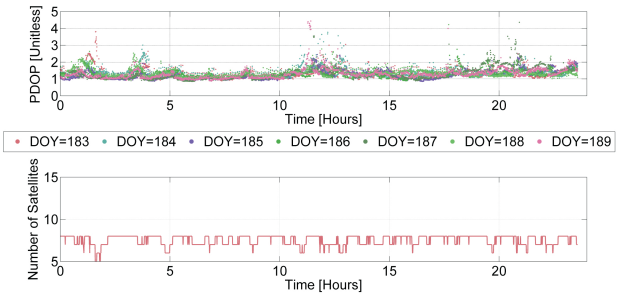

Fig. 20. The PDOP (upper plot) and the number of satellites (lower plot) for DOY 183-189 of 2012 for the site JPLM.

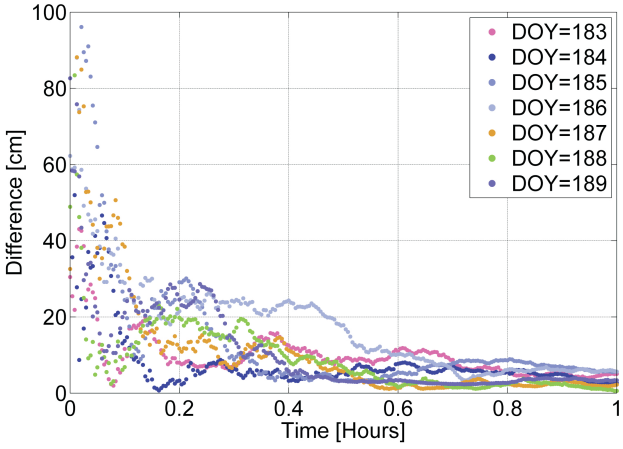

Fig. 21. Site AZU1 from DOY 183-189 of 2012 showing poor horizontal convergence in static mode.

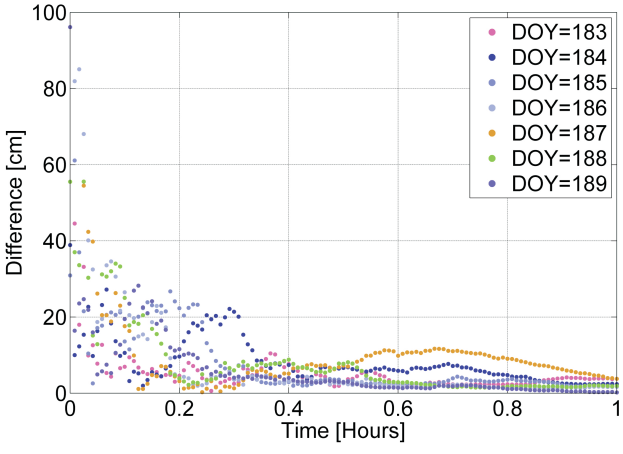

Fig. 22. Site WHC1 from DOY 183-189 of 2012 showing typical convergence in static mode.

presented in (3) and on L_2 (mp_2) in (4),

$$mp_1 = P_1 - \left(1 + \frac{2}{\alpha - 1}\right) L_1 + \left(\frac{2}{\alpha - 1} - 1\right) L_2 \quad (3)$$

$$mp_2 = P_2 - \left(\frac{2\alpha}{\alpha - 1}\right) L_1 + \left(\frac{2\alpha}{\alpha - 1} - 1\right) L_2 \quad (4)$$

where P_1 is the measured pseudorange on L_1 (m), P_2 is the measured pseudorange on L_2 (m), f_1 is the L_1 frequency, and

$$\alpha = \left(\frac{f_1}{f_2}\right) \quad (5)$$

with frequencies $f_1 = L_1$ frequency 1.5754 GHz and $f_2 = L_2$ frequency 1.2275 GHz.

This combination primarily contains pseudorange multipath and noise with no possible distinction between them, plus one constant component associated with carrier-phase ambiguities, and one component associated with instrumental delays.

Under the conditions that (1) multipath and noise have a zero-mean during a period T_m, (2) the hardware delays are constant during T_m and (3) no cycle-slips occur during T_m. The multipath and noise can be obtained through (6) and (7) as,

$$MP1 = mp_1 - mp_{1T_m} \quad (6)$$

$$MP2 = mp_2 - mp_{2T_m} \quad (7)$$

where mp_{1T_m} and mp_{2T_m} is the average of mp_1 and mp_2 respectively, over the period T_m. The average is removed in order to eliminate the constant components. The quantity $MP1$ and $MP2$ contains the white noise components and multipath components with periods smaller than T_m. The mp_{1T_m} and mp_{2T_m} terms are dual-frequency carrier-phase biased combination, due to the inclusion of both L_1 and L_2 in the calculation of $MP1$ and $MP2$. The limitations on the use of this technique include: multipath is not actually a zero mean phenomena, and the pseudorange multipath observable also includes the carrier-phase multipath and noise.

Presented in Figure 23 is the standard deviation of the pseudorange multipath observable for all satellites on DOY 183 of 2012. The standard deviation was calculated by binning the pseudorange multipath observables within an elevation angle bin size of 10°. The stations were arranged based on the standard deviation of the initial bin 10° - 20°. Within the 10° - 20° bin, the site that was prone to the most multipath was AZU1 with a standard deviation of 0.9 m. The site with the least multipath was at JPLM with a value of 0.3 m. As expected, the magnitude of pseudorange multipath decreased as the elevation angle increased.

Brought to you by | York University Libraries
Authenticated
Download Date | 6/18/19 9:37 PM

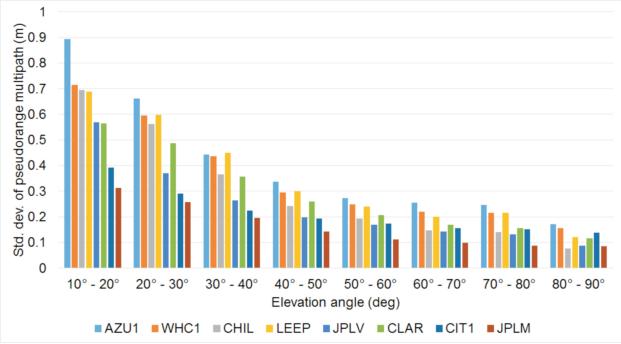

Fig. 23. Standard deviation of the pseudorange multipath observables with a 10° bin size, for all satellites, on DOY 183 of 2012 for the selected 8 IGS sites within the city of Los Angeles.

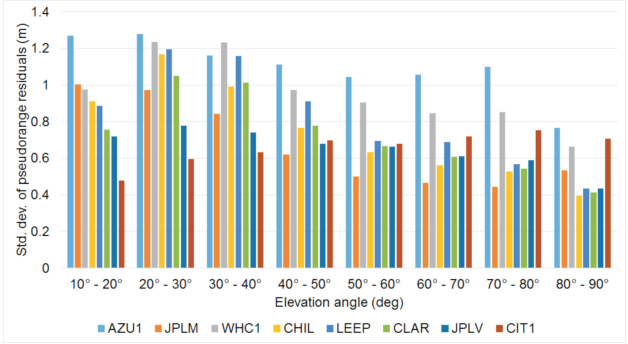

Fig. 25. Standard deviation of the pseudorange residuals with a 10° bin size, for all satellites, on DOY 183 of 2012 for the selected 8 IGS sites within the city of Los Angeles.

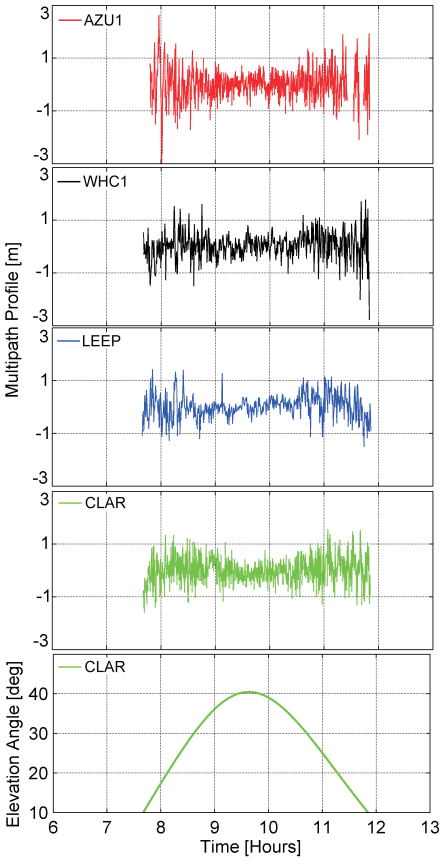

Fig. 24. Comparing the pseudorange multipath profile for PRN 03 at AZU1, WHC1 and CLAR, for DOY 183 of 2012 for the selected IGS sites within the city of Los Angeles. Stations are arranged based on magnitude of standard deviation of the pseudorange multipath and noise observable.

The most consistent trend were at the sites AZU1, CLAR and LEEP where monuments were "shallow rods". Typical of lower cost monuments such as shallow rods, they may tend to be situated in areas such as urban canyons where insufficient room is available to construct permanent and stable monuments such as pillars, as a result, the antenna would be prone to increased multipath.

Illustrated in Figure 24 is the pseudorange multipath observable for PRN 03 for the sites AZU1, WHC1, CLAR and LEEP. For PRN 03, at the site AZU1 had the largest standard deviation of 62 cm followed by WHC1, LEEP and CLAR with standard deviations of 58, 57 and 47 cm respectively. The standard deviation values were calculated based on all data collected from PRN 03 between 7.5 hours and 12 hours GPS time. This trend was observed for all satellites indicating multipath may not be the primary factor for poor initial convergence at AZU1 and CLAR.

The pseudorange residuals were arranged based on the elevation angle. The standard deviation of all satellites were calculated for each elevation bin size of 10°. The standard deviation of the pseudorange observables are illustrated in Figure 25. The stations were arranged based on the standard deviation of the initial bin 10° - 20°. Within the initial bin 10° - 20°, AZU1 had the largest standard deviation of the pseudorange residuals of 1.25 m with minimal improvement up to 80°. At the 80° - 90° bin, the standard deviation of the pseudorange residuals reduced to 0.76 m. Within the initial bin 10° - 20°, CIT1 had the smallest standard deviation of the pseudorange residuals of 0.47 m. As the elevation angle at CIT1 increased, the standard deviation of the pseudorange residuals also increased to a maximum at 80° - 90° bin of 0.70 m. All other stations except AZU1 and CIT1 illustrated the expected trend of a de-

Brought to you by | York University Libraries
Authenticated
Download Date | 6/18/19 9:37 PM

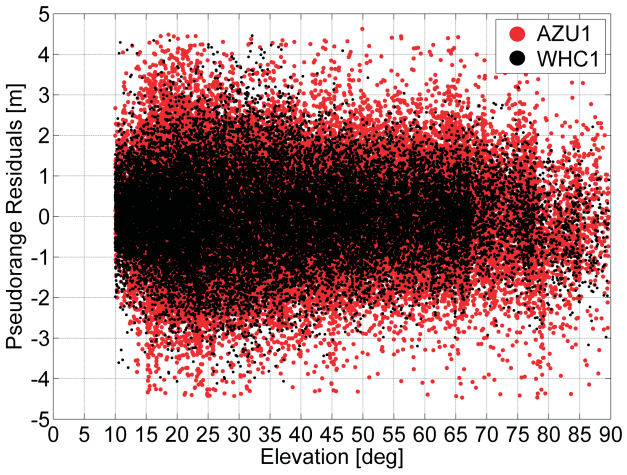

Fig. 26. Comparing the pseudorange residuals for the sites AZU1 (red) and WHC1 (black) for all satellites, for DOY 183 of 2012.

crease in the standard deviation of the pseudorange residuals as the elevation angle increased.

Presented in Figure 26 is an overlay of the pseudorange residuals of all satellites for the sites AZU1 and WHC1. 95% of the residuals of WHC1 ranged between ± 2.13 m with a standard deviation of 0.670 m while at AZU1 95% of the residuals were between ± 2.42 m with a standard deviation of 0.76 m.

Factors examined included monument type and receiver, antenna and clock type for each of the stations, geometric measurement strength, pseudorange multipath and noise and pseudorange residuals. For the 8 sites examined within the Los Angeles area, correlation between pseudorange multipath and noise and the quality of the PPP convergence was observed, which is also reflected in the distribution of the pseudorange residuals. No clear correlation was found between the metrics examined and the final estimated solution.

4 Conclusions and future work

Current limitations of PPP such as the relatively long initial convergence time, pseudorange multipath and noise mitigation, unrealistic position uncertainty and quality of the current PPP models was discussed. The primary factor affecting the initial convergence period of PPP is the quality of the pseudorange measurements. The accuracy of PPP is due to the limited precision of the current precise orbit and clock products and the quality of the models used for atmospheric modelling (primarily the estimation process of the zenith tropospheric delay), the solid Earth tides and ocean loading and pseudorange and carrier-phase multipath and noise. Also presented is the PPP error budget and some of the challenges in defining the error budget as the error sources can be subdivide into errors projected onto the range and localized antenna displacements.

The current accuracy of conventional PPP was assessed by processing GPS data from 300 IGS stations observed during DOY 183 to 189 in 2012. IGS accumulated weekly IGS SINEX station coordinates was used as the reference solution. In static mode, with a data arc of 24 hours, the accuracy was 7 and 13 mm in the horizontal and vertical components, respectively. In kinematic mode, with a data arc of 24 hours, the conservative accuracy of the horizontal component was 46 mm and 72 mm in the vertical component. The solution quality deteriorated because of the magnitude of the process noise used, adding large uncertainties to each parameter, allowing the solution to converge freely based on individual measurements. Whereas, in static mode the parameters are tightly constrained, thus a significantly higher accuracy of results is achieved through the power of averaging.

A horizontal threshold of 20 cm was set to examine the amount of time required for 95% of the data processed to attain this pre-defined threshold. A threshold of 20 cm was selected as this specification is utilized in a variety of commercial applications such as offshore positioning for hydrography (dynamic positioning, construction, etc.), precision agriculture, and airborne mapping for aircraft / camera sensor positioning. Conventional solutions are slow to converge, with approximately 20 minutes required for 95% of solutions to reach the 20 cm or better horizontal accuracy in static mode and it took 55 minutes for 89% of data, in kinematic mode. It would be recommended, based on the results processed, to collect an initial 20 minutes of data while the receiver is stationary, after which the receiver can be switched to kinematic mode and moved to collect data at various locations.

Also examined is the geographic distribution of the positional biases. 5% of the estimated PPP solutions with largest differences from the IGS SINEX solutions were most noticeable in regions such as South America, Asia and southern Africa where the IGS has a weaker densification of continuously operating reference stations and around coastal regions. Also, some South American stations may be affected by more active ionospheric conditions.

Factors that possibly affect quality of convergence were examined within a test site located in Los Angeles consisting of 8 active control points. Some of the factors examined include monument type and receiver, antenna

Brought to you by | York University Libraries
Authenticated
Download Date | 6/18/19 9:37 PM

and clock type for each of the stations. Also analysed was the geometric measurement strength, pseudorange multipath and noise and pseudorange residuals. It's also noted, the sensitivity of the receiver and its effects on the quality of the PPP convergence and final solution. Correlation between pseudorange multipath and noise and the quality of the PPP convergence was observed, which is also reflected in the distribution of the pseudorange residuals. No clear correlation was found between the metrics examined and the final estimated solution.

Further analysis is required to determine if there is a root cause or causes of these solution variations, or if the variations reflect the limits of the processing technique. Additional work would also include upgrading the York-PPP software to process GLONASS and Galileo data, as well as work on the functionality of the software to allow for a real-time solution as real-time IGS data streams are now publically available.

Acknowledgement: The research was funded from the Natural Sciences and Engineering Research Council of Canada. The results presented are derived from data and products provided by Natural Resources Canada and the International GNSS Service.

References

[1] Bisnath S. and Gao Y., Current State of Precise Point Positioning and Future Prospects and Limitations, *International Association of Geodesy Symposia – Observing our Changing Earth* 133, (2008), 615-623.

[2] Bisnath S. and Collins P., Recent Developments in Precise Point Positioning, *GEOMATICA* 66(2), (2012), 103-11.

[3] CDDIS (2013) Crustal Dynamics Data Information System, ftp://cddis.gsfc.nasa.gov/pub/gps/, accessed: 2013.

[4] Collins P., Isolating and Estimating Undifferenced GPS Integer Ambiguities, *Proc. ION NTM* (2008), 720-732.

[5] Official U.S. Government information about the Global Positioning System (GPS) and related topics, New Civil Signals, http://www.gps.gov/systems/gps/modernization/civilsignals/, accessed: 2013.

[6] Eckl M., Snay R., Soler T., Cline M. and Mader G., Accuracy of GPS-Derived Relative Positions as a Function of Interstation Distance and Observing-Session Duration, *Journal of Geodesy* 75(12), (2001), 633-40.

[7] Elsobeiey M. and El-Rabbany A., Rigorous Modelling of GPS Residual Errors for Precise Point Positioning, *Proceedings of the 2010 Canadian Geomatics Conference*, Calgary, (2009), 80-194.

[8] Wide-area Augmentation System Performance Analysis Report, Report No. 42, (2012), 172.

[9] Geospatial Positioning Accuracy Standards, Part 3: National Standard for Spatial Data Accuracy, The Federal Geographic Data Committee, Report No. FGDC-STD-007.3-1998, (1998), 25.

[10] Ge M., Gendt G., Rothacher M., Shi C. and Liu J., Resolution of GPS Carrier-Phase Ambiguities in Precise Point Positioning (PPP) with Daily Observations, *Journal of Geodesy* 82(7), (2008), 389-99.

[11] Geng J., Meng X., Dodson A. H. and Teferle F. N., Integer Ambiguity Resolution in Precise Point Positioning: Method Comparison, *Journal of Geodesy* 84(9), (2010), 569-81.

[12] Hernández-Pajares M., Juan J. M., Sanz J., and Orús R., Second-order ionospheric term in GPS: Implementation and impact on geodetic estimates, *Journal of Geophysical Research* 112(B8), (2007), 2156-2202.

[13] Hofmann-Wellenhof B., Lichtenegger H., and Collins J., *GPS Theory and Practice*, 5th edn. New York: Springer-Verlag Wien, (2001), 389.

[14] Héroux P., and Kouba J., GPS Precise Point Positioning with a Difference, *Geomatics'95*, June 13-15, (1995), Ottawa, Canada.

[15] IGS Products, The International GNSS Service (IGS), http://igscb.jpl.nasa.gov/components/prods.html, accessed: 2013.

[16] Manual on Hydrography, 1st edn. International Hydrographic Bureau, (2005), 32.

[17] Kouba J., *A guide to using International GNSS Service (IGS) products*, (2009), http://igscb.jpl.nasa.gov/igscb/resource/pubs/UsingIGSProductsVer21.pdf, accessed: 2013.

[18] Kouba J. and Héroux P., Precise Point Positioning using IGS Orbit and Clock Products, *GPS solutions* 5(2), (2001), 12-28.

[19] Laurichesse D., Mercier F., Berthias J., Broca P. and Cerri L., Integer Ambiguity Resolution on Undifferenced GPS Phase Measurements and its Application to PPP and Satellite Precise Orbit Determination, *Navigation* 56(2), (2009), 135-149.

[20] Leandro R. F., *Precise Point Positioning with GPS: A New Approach for Positioning, Atmospheric Studies, and Signal Analysis*, Ph. D. dissertation,University of New Brunswick, Canada, (2009), 203.

[21] Li W., Yuan Y., Ou J., Li H., and Li Z., A New Global Zenith Tropospheric Delay Model IGGtrop for GNSS Applications, *Chinese Science Bulletin* 57(17), (2012), 2132-9.

[22] Mireault Y., Tétreault P., Lahaye F., Héroux P. and Kouba J., Online Precise Point Positioning, *GPS World* 19(9), (2008), 59-64.

[23] About Us, Natural Resources Canada, http://www.nrcan-rncan.gc.ca/com/index-eng.php, accessed: 2013.

[24] Ochieng W. Y., Sauer K., Walsh D., Brodin G., Griffin S. and Denney M., GPS Integrity and Potential Impact on Aviation Safety, *Journal of Navigation* 56(1), (2003), 51-65.

[25] Petrovski I. G. and Tsujii T., *Digital Satellite Navigation and Geophysics: A Practical Guide with GNSS Signal Simulator and Receiver Laboratory*, 1st edn. Cambridge University Press, (2012), 338.

[26] Scherneck H., Ocean Tide Loading Provider, http://froste.oso.chalmers.se/loading//index.html, accessed: 2013.

[27] Seepersad G., and Bisnath S., Integrity Monitoring in Precise Point Positioning, *Proceedings of the 26th International Technical Meeting of The Satellite Division of the Institute of Navigation* (ION GNSS 2013), Nashville, TN, (2013), 1164-1175.

[28] Seepersad G. and Bisnath S., Reduction of Precise Point Positioning Convergence Period, *Proceedings of the 25th International Technical Meeting of The Satellite Division of the Institute of Navigation* (ION GNSS 2012), Nashville, TN, (2012), 3742-3752.

Brought to you by | York University Libraries
Authenticated
Download Date | 6/18/19 9:37 PM

[29] Seepersad G., *Reduction of Initial Convergence Period in GPS PPP Data Processing*, M. Sc. dissertation,York University, Toronto, Ontario, (2012), 131.

[30] Wang J. and Feng Y., Integrity Determination of RTK Solutions in Precision Farming Applications, *Proceedings of the Surveying and Spatial Sciences Institute Biennial International Conference* 2009, Surveying and Spatial Sciences Institute, (2009), 1277-1291.

[31] Wells D. E., Beck N., Delikaraoglou D., Kleusberg A., Krakiwsky E., Lachapelle G., Langley R., Nakiboglu M., Schwarz K. and Tranquilla J., *Guide to GPS Positioning*, Department of Geodesy and Geomatics Engineering, Lecture Note No. 58, University of New Brunswick, NB, Canada, (1999), 601.

[32] Zumberge J., Heflin M., Jefferson D., Watkins M. and Webb F., Precise Point Positioning for the Efficient and Robust Analysis of GPS Data from Large Networks, *Journal of Geophysical Research* 102(B3), (1997), 5005-17.

Brought to you by | York University Libraries
Authenticated
Download Date | 6/18/19 9:37 PM